Journal of the European Ceramic Society 17 (1997) 859–864

PII: S0955-2219(96)00160-4
0955-2219/97/$17.00

Creep Behaviour of Alumina, Zirconia and Zirconia-Toughened Alumina

J. Chevalier, C. Olagnon, G. Fantozzi & H. Gros

G.E.M.P.P.M., UMR C.N.R.S. 5510, I.N.S.A. Bât. 502, 69621 Villeurbanne, France

(Received 18 April 1996; revised version received 22 July 1996; accepted 5 August 1996)

Abstract

Creep behaviour of various alumina, zirconia and zirconia-toughened alumina is investigated. A very large scale of creep rates and creep behaviours is observed. Creep rate depends on the grain size, on the purity and on the composition of the glassy phase present in grain boundaries. Cavitation and microcracking by grain boundary sliding have been identified as the main creep mechanisms. © 1997 Elsevier Science Limited. All rights reserved.

1 Introduction

The deformation of alumina ceramics at high temperatures has been extensively reported in literature.[1] The dependence of steady-state creep rate on stress, temperature and grain size is given by a general relationship of the form:

$$\dot{\varepsilon} = \frac{ABDGb}{kT} \cdot \left(\frac{b}{d}\right)^m \cdot \left(\frac{\sigma}{G}\right)^n \qquad (1)$$

where A is a constant, D is the diffusion coefficient, G the shear modulus, b the Burgers vector, k the Boltzmann's constant, T the absolute temperature, d the grain size, σ the applied stress and m and n the grain size and stress exponents respectively. The diffusion coefficient is given by:

$$D = D_0 \exp(-Q/RT) \qquad (2)$$

with D_0 a frequency factor, Q the activation energy for the diffusion process and R the gas constant.

The values obtained experimentally for m, n and Q on alumina polycrystals are in the range: $0 \leq m \leq 3$, $0{\cdot}7 \leq n \leq 3{\cdot}30$, $295 \leq Q \leq 840$ kJ mol^{-1}.

For polycrystals, the rate-controlling creep mechanisms are of two types: intragranular (i.e. lattice mechanisms independent of the grain size so that $m = 0$) and those involving the grain boundaries (boundary mechanisms where m is in the range of 1 to 3). There is a large number of mechanisms[1] for which the predicted values for the exponents m and n can be determined. Theoretically, it is possible to identify creep mechanisms from analysis of creep data (m, n, Q, D_0) and so to obtain a deformation mechanism map[2,3] as a function of stress, temperature and grain size. However, in practice this identification is difficult because the mechanisms depend on both microstructure and chemical composition of materials and two or more mechanisms can occur. The different mechanisms observed for alumina polycrystals are the following: lattice mechanisms (dislocation creep models),[4] diffusion creep[4–6] (Nabarro–Herring and Coble creep), interface reaction controlled diffusion creep,[7] grain boundary sliding,[2,4,5] cavitation creep and microcracking.[8]

The main objective of this paper is to study the creep behaviour of zirconia-toughened alumina in order to understand the influence of zirconia on the creep behaviour of alumina-based composites. In order to have a better understanding of the creep behaviour of the ceramic composites, creep characteristics of monolithic alumina and zirconia are first studied.

2 Materials and Experimental Procedure

Alumina, zirconia and zirconia-toughened alumina were prepared by C T. Desmarquest. They were prepared by mixing the different raw materials in water with a deflocculant. The suspension was homogenized by ball milling and the dispersion was achieved by ultrasonication. Small pellets were then shaped by slip casting in a plaster mould. High green densities (55 to 60%) were obtained. The green parts were then pressureless sintered in air. In some cases, after pressureless sintering, a hot isostatic pressing (HIP) was conducted. Table 1 gives the composition and preparation details of the 11 studied materials.

Table 1. Designation, composition and flexural strength of studied materials, and creep parameters Q and n

Ceramic system	*Nomenclature, preparation conditions*	*Composition*	σ_f *at RT (MPa)*	Q *(kJ/mol)*	n
Alumina	A1, sintered 1600°C	Purity > 99·98%	415 ± 10	630 ± 10	2·5 ± 0·2
	A1g, sintered 1650°C	Purity > 99·98%	470 ± 20	650 ± 20	
	A3	Purity > 99·98% 1000 ppm MgO	380 ± 20	630 ± 10	
Zirconia	Z1, sintered 1750°C	Mg PSZ 3% wt MgO, purity > 99·9%	410 ± 40		
	Z5, sintered 1750°C	Mg PSZ 3% wt MgO, purity > 99·6%	620 ± 20		
	ZFME, sintered 1750°C	Mg PSZ 4% wt MgO	375 ± 5		1·4 ± 0·2
	ZFYT	TZP 3% mol Y_2O_3	1000 ± 20		
Zirconia-toughened alumina	A1-10Z1, sintered 1600°C	Al_2O_3:A1 10% vol ZrO_2:Z1	540 ± 20	760 ± 20	2·5 ± 0·2
	A1-10ZY3, sintered 1600°C	Al_2O_3:A1 10% vol ZrO_2: Z1 3% mol Y_2O_3	430 ± 20		
	A1-10Z4, sintered 1600°C	Al_2O_3: A1 10% vol finer ZrO_2 (Z4)	550 ± 20		
	A2-10Z1, sintered 1600°C	Al_2O_3:A2 purity > 99·6% 1000 ppm MgO 10% vol ZrO_2 Z1	480 ± 5		

2.1 Alumina

Two alumina powders were used: the first, used for the preparation of A1 and Alg, was purer than the second (used for A3) containing 1000 ppm of MgO. The A3 powder also contained more SiO_2 (0·06 wt% against 0·02 wt% for A1) and Na_2O (0·16 wt% against 0·05 wt%). The microstructures of the A1, Alg and A3 aluminas were very similar, with a mean grain size of 2·7 μm for A1, 3·5 μm for Alg (grain size slightly higher than that of A1 as a consequence of the higher temperature sintering) and 2·4 μm for A3. The A3 alumina had a higher porosity content and a slightly smaller average grain size due to the presence of MgO.

2.2 Zirconia

Three MgO- and one Y_2O_3-doped zirconia ceramics were studied.

For MgO-doped zirconia (MgPSZ), three powders with different purities were used: the first (Z1) was the purer, with 0·001 wt% SiO_2, 0·03 wt% Al_2O_3 and 0·006 wt% TiO_2. The second (Z5) contained 0·02 wt% SiO_2, 0·07 wt% Al_2O_3 and 0·11 wt% TiO_2. The third (ZFME) was developed from a powder with a rather high SiO_2 content (0·2 wt%).

The microstructures were typical of partially stabilized zirconia, consisting of large cubic grains (≅ 50 μm for Z1 and Z5, 100 μm for ZFME) with monoclinic and tetragonal precipitates at grain boundaries and inside cubic phase grains.

ZFYT was a tetragonal zirconia polycrystals zirconia containing 3 mol% Y_2O_3 with a low grain size of about 0·5 μm.

2.3 Zirconia-toughened alumina

Four zirconia-toughened aluminas (ZTA) were prepared.

The first, designated A1-10Z1 in the nomenclature, was prepared with the alumina A1 powder and 10 vol% of zirconia Z1 powder, and sintered at 1600°C. The second, A1-10ZY3, was prepared with the same powders, with an addition of 3 mol% Y_2O_3. The microstructure of these two ZTA consisted of a homogeneous dispersion of zirconia particles (≅ 0.5 μm) located at grain junctions of alumina grains (≅ 2 μm).

The third ZTA (A1-10Z4) was prepared with the same alumina base, but a different zirconia powder (Z4), finer than Z1, was used. This resulted in finer zirconia particles (≅ 0·3 μm), but the presence of some zirconia particle agglomerates of about 2 μm was observed.

Finally, the A2-10Z1 ceramic was prepared from an alumina powder (A2) with a low purity (less pure than A3) containing 1000 ppm of MgO, and from the Z1 zirconia powder. The microstructure of this ZTA was similar to that of A1-10Z1 and A1-10ZY3.

2.4 Experimental procedure

Mechanical tests were conducted in four-point bending on bar-shaped specimens with dimensions of about 3 × 4 × 40 mm^3. The tensile face of the specimens was polished with diamond paste (6 μm and 1 μm) and the edges were chamfered (about 45°). The parallelism of top and bottom surfaces was strictly controlled (about 0·01 mm).

Flexural strengths were measured at room temperature with a four-point bending fixture with 36 mm outer span and 18 mm inner span.

Creep tests were carried out in air at temperatures up to 1400°C under stresses from about 50 to 200 MPa, with the same four-point bending fixture as for flexural strengths. The heating rate was low enough (about 300°C/h) to avoid any significant thermal gradients and so thermal instabilities. In order to obtain dimensional stability of all parts of the creep machine, the system was maintained for one hour at the operating temperature before creep tests. Then load was increased uniformly to the nominal value. During the test, variations of specimen deflection (measured at the centre of the beam), applied load and specimen temperature were recorded as functions of time.

The flexural stress on the sample tensile face was calculated by the expression:

$$\sigma = \frac{3P(L - l)}{2Bw^2} \tag{3}$$

with P the applied load, L the outer span, l the inner span, B the specimen width and w the specimen thickness.

The creep strain was calculated from the deflection y_c at the centre of the beam using the method of Hollenberg *et al.*:[9]

$$\varepsilon = K(n)y_c \tag{4}$$

with

$$K(n) = \frac{2w(n + 2)}{(L - l)[n + 1] + l^2(n + 2)/2} \tag{5}$$

The constant $K(n)$, in addition to its dependence on n, is also a function of the spans (L and l). Hollenberg *et al.* have shown that for (L/l) ratio values close to 2, $K(n)$ is almost insensitive to the n value. So, expression (5) can be used and ε calculated with an approximate value for n. In case of a too high divergence between the determined n and the initial supposed n, calculations of ε must be made again.

3 Results

Figure 1 represents the steady-state creep rate (in the secondary creep stage) of the 11 ceramics at 1200°C under a stress of 100 MPa.

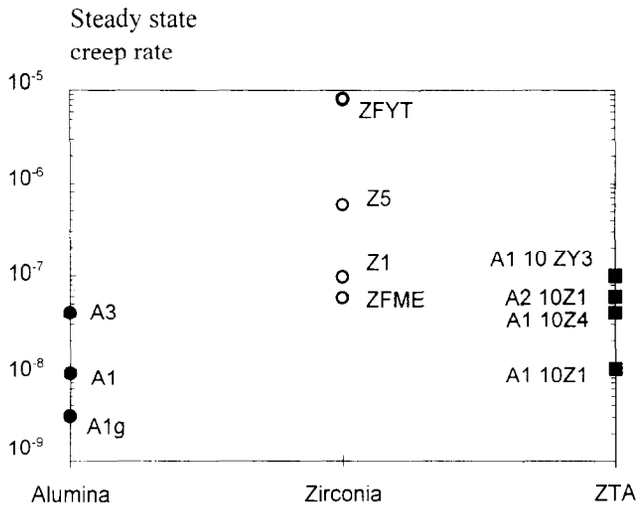

Fig. 1. Steady-state creep rates of the 11 ceramics at 1200°C, 100 MPa.

3.1 Creep behaviour of alumina

The effect of grain size for the two A1 powder-based aluminas is clear from the decrease of creep rate as the grain size increases ($\dot{\varepsilon} \cong 9{\cdot}10^{-9}$ s^{-1} for A1 and $3{\cdot}10^{-10}$ s^{-1} for A1g). It appears that the alumina A1 with the finer grain size has the lower creep resistance, which is in agreement with expression (1). Figure 1 also shows that the quasi-steady-state creep rate is higher when the purity is lower (comparison between the A1 and A3 aluminas): $\dot{\varepsilon} \cong 9{\cdot}10^{-9}$ s^{-1} for A1 and $4{\cdot}10^{-8}$ s^{-1} for A3.

The stress exponent n and the activation energy Q of eqns (1) and (2) were determined for the different alumina materials from the results obtained at different temperatures. The isothermal method was used for the measurement of Q. The log of steady-state creep rate was plotted versus $1/T$ as shown in Fig. 2. The activation energies were obtained from the slope of the straight lines in Fig. 2 and are listed in Table 1. The activation energy values are very similar and in good

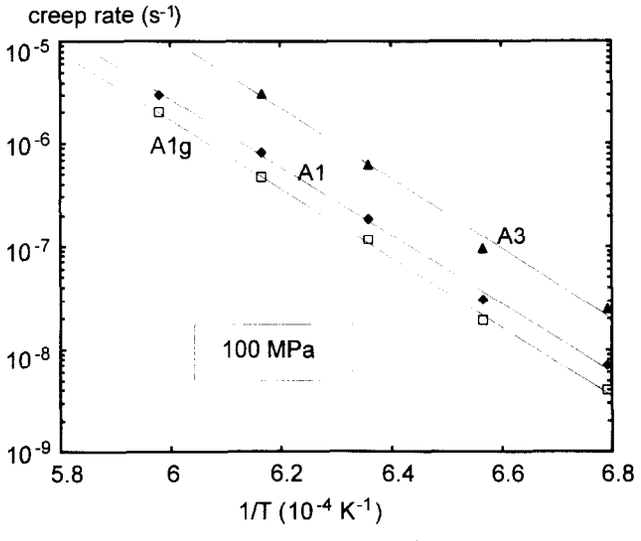

Fig. 2. Steady-state creep rate versus $10^4/T$ with σ = 100 MPa for A1, A1g and A3 alumina.

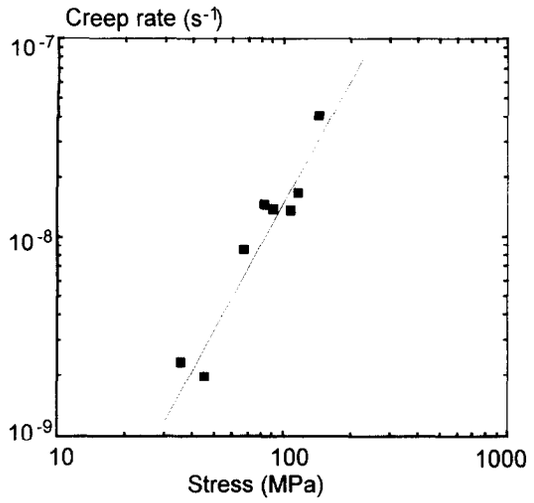

Fig. 3. Steady-state creep rate as a function of stress at 1200°C for A1 alumina.

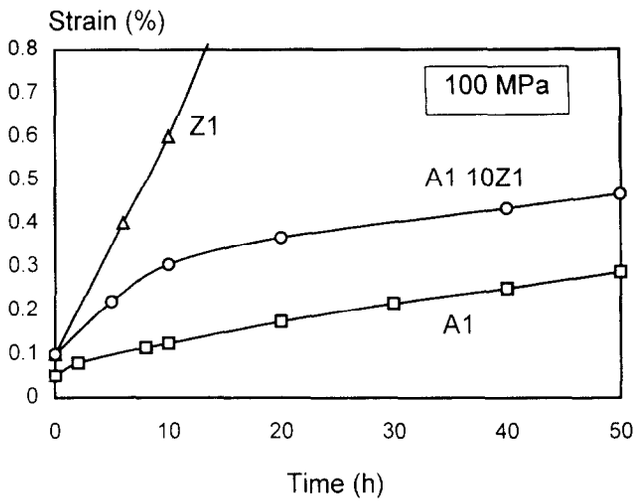

Fig. 4. Creep curves of A1 alumina, Z1 zirconia and A1-10Z1 zirconia-toughened alumina at 1200°C, 110 MPa.

agreement with values reported previously.[7] The stress exponent n was determined by studying the variation of the creep rate as function of the applied stress (Fig. 3) at a given temperature of 1200°C. n is calculated from the slope of the straight line of Fig. 3 by using the least-squares method. The plot yields $n = 2{\cdot}5 \pm 0{\cdot}2$ for A1 alumina at 1200°C.

3.2 Creep behaviour of zirconia

The TZP ceramic (ZFYT) presents a poor creep resistance.

For the PSZ materials, different behaviours can be noticed. The effect of purity on creep behaviour is clear from the lower creep resistance of Z5 as compared to Z1 (Z1 and Z5 have the same grain size, but Z1 is purer): $\dot{\varepsilon} \cong 1{\cdot}10^{-7}$ s^{-1} for Z1 and $6{\cdot}10^{-7}$ s^{-1} for Z5.

The effect of microstructure can be stated by the highest creep resistance of the ZFME ceramics ($\dot{\varepsilon} \cong 6{\cdot}10^{-8}$ s^{-1}) which has the coarsest microstructure. It appears that, like alumina, creep resistance is favoured by a large grain size.

The stress exponent n has been measured for the ZFME zirconia by the same procedure as for the A1 alumina. The results gave $n = 1{\cdot}4 \pm 0{\cdot}2$.

3.3 Creep behaviour of zirconia-toughened alumina

Different behaviours can be observed as can be seen from a large range of creep resistances. The lowest creep rate is obtained for the A1-10Z1 composite. Addition of yttria-stabilized zirconia increases the creep rate as shown by the results on A1-10ZY3.

The presence of agglomerates of zirconia particles (A1-10Z4) is detrimental. Finally, the purer the alumina powder, the lower the creep rate (the creep rate of A2-10Z1 composite is six times higher than the creep rate of A1-10Z1 ZTA).

Furthermore it was also observed that the A2-10Z1 ceramics presented a large primary creep stage.

If we compare the creep behaviour of the A1-10Z1 composite with that of the matrix A1 (Figs 1 and 4), it can be noticed that the steady-state creep rates of the two ceramics are very similar ($\dot{\varepsilon} \cong 10^{-8}$ s^{-1}). But it is also observed that the total strain is lower for A1 alumina because of a lower first-stage creep rate. The comparison with the Z1 zirconia shows that creep resistance of A1-10Z1 is higher than for Z1 alone.

The activation energy and the stress exponent were determined for the A1-10Z1 ceramic by conducting tests at different temperatures and stresses. These are listed in Table 1. We must note that the stress exponent is similar to that of the A1 one ($n \cong 2{\cdot}5$).

4 Discussion

Scanning and Transmission Electron Microscopy (SEM and TEM respectively) have been conducted to characterise the evolution of the microstructure after creep tests. In the case of alumina creep samples, we have essentially examined the A1 alumina.

A micrograph of the material after creep at 1400°C is shown in Fig. 5: small cavities (A) appear at triple grain junctions and along grain boundaries, cavity growth (B) and facet-sized cavity (C) can be noticed. This microstructure is typical of a boundary cavitation with glassy phase. The presence of a glassy phase has been confirmed by TEM observations (Fig. 6): this glassy phase appeared as a thin film of about 1 nm along the grain boundaries and as pockets at triple junctions. These TEM observations equally showed that after

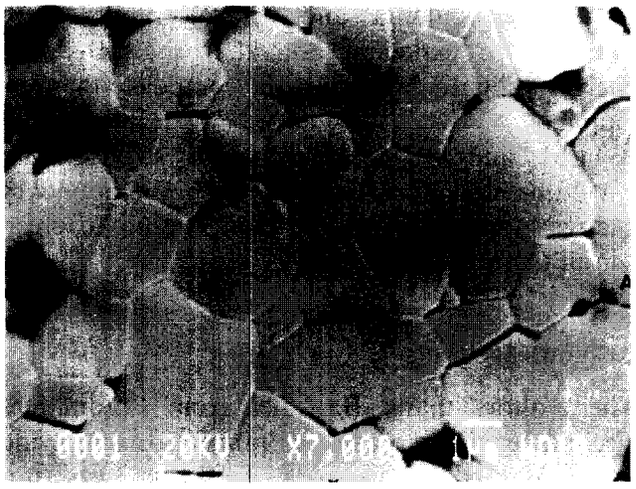

Fig. 5. Microstructure of A1 alumina crept at 1400°C (ε = 2·6%), showing small cavities at grain boundary (A), cavity growth (B) and cavity facets (C).

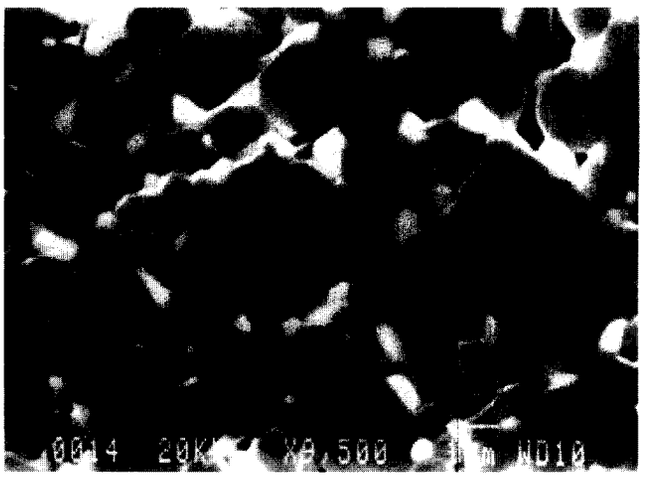

Fig. 7. Microstructure of A1-10Z1 composite crept at 1200°C, showing the presence of numerous cavities.

creep at 1400°C, growth of cavities occurred rather than nucleation. Note that no grain growth was observed. At 1200°C, a higher density of smaller cavities was observed, indicating a continuous nucleation of cavities with no significant growth.

Damage due to microcracking induced by creep has been evaluated by measuring flexural strength at room temperature on crept samples. For the A1 alumina, the flexural strength decreases from 415 ± 10 MPa to 330 ± 20 MPa after creep at 1200°C. The defect size increase due to creep can be estimated from this variation at about 1·6.

In the case of the PSZ ceramics significant macroscopic damage was observed after creep: many long cracks appear on all the faces of the sample. SEM observations showed that cracking occurs along the grain boundaries and that the damage was homogeneously distributed within the sample. On the contrary, TZP ceramics do not show macroscopic damage but cavities, holes and cracks clearly appear during SEM observations. Cracks were preferentially perpendicular to the traction axis. It can be considered that a general cavitation mechanism occurs with nucleation, growth and coalescence of cavities which leads to the formation of holes and then of cracks.

Concerning the ZTA ceramics, cavitation first appears at triple grain junctions (Fig. 7) as for alumina and, as already observed by Wang *et al.*,[10] grain boundary decohesion and facet-sized cavitation occur, which leads to microcracking particularly at alumina–alumina and alumina–zirconia boundaries perpendicular to the applied stress. After creep at 1200°C, the cavities and facet-sized numbers were higher for the ZTA materials than for alumina. This could explain the higher creep strain noticed for ZTA, essentially during the primary creep stage.

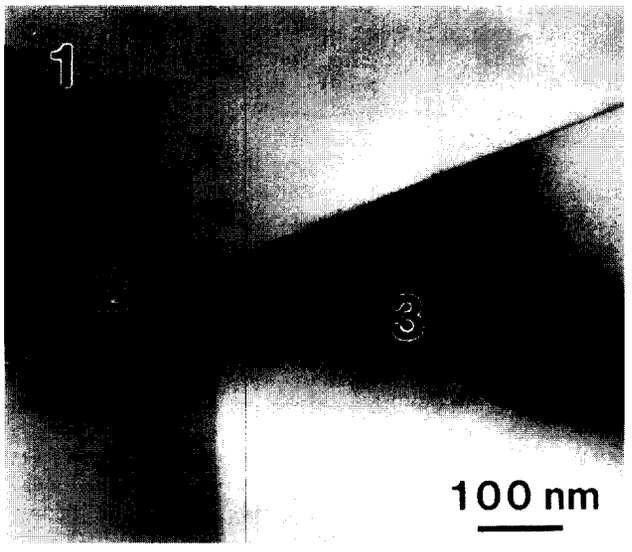

(a)

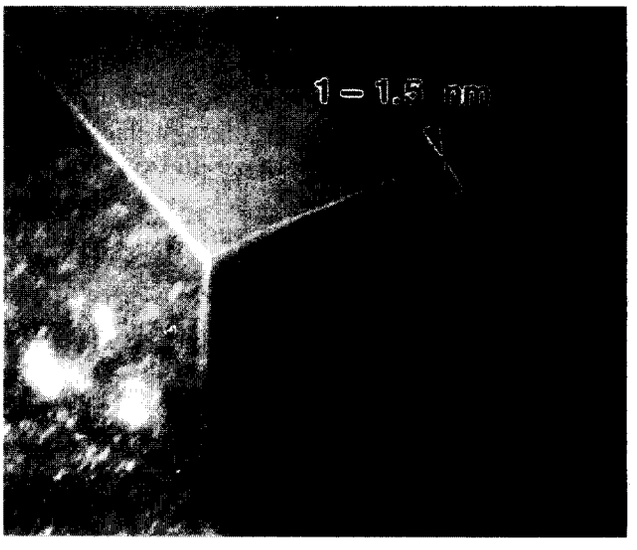

(b)

Fig 6. Bright field (a) and dark field (b) TEM pictures, indicating the presence of a thin vitreous phase at grain boundary.

We have observed that the addition of yttria to PSZ increases the creep rate as shown in Fig. 1 (comparison between A1-10Z1 and A1-10ZY3). The microstructure of the two ceramics is very similar. Therefore, we can suppose that the grain boundary glassy phase changes with the yttria content, perhaps because yttria segregates partly at grain boundary. This hypothesis should be verified by TEM and analysis observations but is often made for TZP ceramics.[11,12]

The effect of cavitation on creep has been studied by Riedel and Rice.[13,14] The creep rate is given by the following relation:

$$\varepsilon = \varepsilon_s + N\left(\frac{2\pi r^2}{X}\right)\frac{2\Omega\delta D_b\sigma}{kTq(\omega)} \quad (6)$$

where ε_s is the creep rate without cavitation, N the volume density of cavities, r the cavity tip radius, δ the grain boundary thickness, λ the distance between cavities, D_b the grain boundary diffusion coefficient, Ω the atomic volume and $q(\omega) = -2\ln\omega - (3-\omega)(1-\omega)$ with $\omega = (2r/\lambda)^2$.

We have estimated the contribution of cavitation on creep for the A1 alumina by taking the following figures of parameters: $D_b = 2{\cdot}7 \times 10^{-19}$ m^2/s, $\Omega = 4{\cdot}2 \times 10^{-29}$ m^3, $T = 1673$ K, $\sigma = 96$ MPa, $N = 6 \times 10^{13}$ m^{-3} (measured by TEM observations), $r = 0{\cdot}5$ μm, $\lambda = 6$ μm, $\omega = 1/36$, $q(\omega) = 4{\cdot}28$ and $\delta = 10^{-3}$ μm. With these figures, the cavitation contribution to the steady-state creep rate corresponds to about 60%.

The stress threshold σ_c for cavitation can be evaluated by using the Lange[15] or Evans and Rana[16] models. This stress threshold is equal to:

$$\sigma_c = 4\gamma/d \quad (7)$$

where γ is the surface energy of the glassy phase and d the cavity diameter (roughly given by the thickness of the glassy phase).

With the thickness of 1 nm measured by TEM and $\gamma = 0{\cdot}35$ J/m^2 (corresponding to silicate-based glasses), σ_c for A1 alumina is estimated to about 140 MPa. This figure agrees fairly well with our experimental observations of cavitation only for stresses higher than 100 MPa.

5 Conclusion

This study has shown the very large scale of creep rates and creep behaviours that particle-reinforced alumina could exhibit. Creep rate depends on the composition of the glassy phase (viscosity) present in grain boundaries, on the grain size and on the purity. The presence of yttria-stabilized zirconia is not favourable for creep resistance, but its role is not clear and needs to be elucidated. Our results show that alumina and ZTA ceramics have the same n exponent and that the activation energy is slightly higher for the composite than for alumina.

TEM and SEM observations suggest that cavitation and microcracking by grain boundary sliding supply most of the contribution to creep for all the ceramics studied.

Acknowledgements

The authors thank B. Cales from Céramiques Techniques Desmarquest (France) for supplying materials used in this work. This work was supported in part by Brite contract no RI-1B-0202-C.

References

1. Canon, W. R. & Langdon, T.G., Review: creep of ceramics. Part 1: Mechanical characteristics. *J. Mater. Sci.*, **18** (1983) 1–50.
2. Heuer, A. H., Tighe, N. J. & Cannon, R. M., Plastic deformation of fine grained alumina: II, basal slip and non-accommodated grain boundary sliding. *J. Am. Ceram. Soc.*, **63** (1980) 53–58.
3. Cannon, R. M., Rhodes, W. H. & Heuer, A. H., Plastic deformation of fine grained alumina: I, interface controlled diffusional creep. *J. Am. Ceram. Soc.*, **63** (1980) 46–53.
4. Cannon, W. R. & Sherby, O. D., Creep behaviours and grain boundary sliding in polycrystalline Al_2O_3. *J. Am. Ceram. Soc.*, **60** (1977) 44–47.
5. Davies, C. K. L. & Sinha Ray, S. F., High temperature creep deformation of polycrystalline alumina in tension. In *Special Ceramics 5*, ed. P. Popper. British Ceramic Research Association, Stoke on Trent, 1972, pp. 193–209.
6. Passmore, E. M. & Vassilos, T., Creep of dense, pure, fine grained aluminium oxide. *J. Am. Ceram. Soc.*, **49** (1966) 166–168.
7. Chokhi, A. M. & Porter, J. R., High temperature mechanical properties of single phase alumina. *J. Mater. Sci.*, **21** (1986) 705–710.
8. Clarke, D. R., High temperature deformation of a polycrystalline alumina containing an intergranular glassy phase. *J. Mater. Sci.*, **20** (1985) 1321–1332.
9. Hollenberg, G. W., Terwilliger, G. R. & Gordon, R. S., Calculation of stresses and strains in four point bending creep tests. *J. Am. Ceram. Soc.*, **54** (1971) 196–199.
10. Wang, P., Grathwohl, G. & Thümmler, F., *Powder Metallurgy International*, **24** (1992) 365.
11. Stoto, T., Nauer, M. & Carry, C., Influence of residual impurities on phase partitioning and grain growth processes of Y-T2P materials. *J. Am. Ceram. Soc.*, **74** (1991) 2615.
12. McCartney, M. L., Influence of an amorphous second phase on the properties of yttria stabilized tetragonal polycrystals (Y-T2P). *J. Am. Ceram. Soc.*, **70** (1987) 54–58.
13. Riedel, H. & Rice, J. R., Tensile cracks in creeping solids. In *Fracture Mechanics, ASTM STP 700*, American Society for Testing and Materials, 1980, 112–130.
14. Rice, J. R., Constraints on the diffusive cavitation of isolated grain-boundary facets in creeping polycrystals. *Acta Metall.*, **29** (1981) 675–681.
15. Lange, F. F., Non-elastic deformation of polycrystals with a liquid grain boundary phase. *Proc. Symposium on the Plastic Deformation of Ceramic Materials*, Pennsylvania, 17–19 July 1974, ed. R. C. Bradt & R. E. Tressler. Plenum Press, NY, 1975, pp. 361.
16. Evans, A. G. & Rana, A., High temperature failure mechanisms in ceramics. *Acta Metall.*, **28** (1980) 129–141.